

# Pulsed laser deposition of hydroxyapatite on titanium substrate with titania interlayer

P. Rajesh · C. V. Muraleedharan · Manoj Komath ·  
Harikrishna Varma

Received: 9 September 2010 / Accepted: 4 January 2011 / Published online: 14 January 2011  
© Springer Science+Business Media, LLC 2011

**Abstract** Pulsed laser deposition (PLD) has been used to deposit hydroxyapatite (HA) ceramic over titanium substrate with an interlayer of titania. PLD has been identified as a potential candidate for bioceramic coatings over metallic substrates to be used as orthopedic and dental implants because of better process control and preservation of phase identity of the coating component. However, direct deposition of hydroxyapatite on titanium at elevated temperature results in the formation of natural oxide layer along with some perovskites like calcium titanate at the interface. This leads to easy debonding of ceramic layer from the metal and thereby affecting the adhesion strength. In the present study, adherent and stable HA coating over Ti6Al4V was achieved with the help of an interlayer of titania. The interlayer was made to a submicron level and HA was deposited consecutively to a thickness of around one micron by exposing to laser ablation at a substrate temperature of 400°C. The deposited phase was identified to be phase pure HA by X-ray diffraction, scanning electron microscopy, energy dispersive X-ray analysis, and inductively coupled plasma spectrometry. The mechanical behavior of coating evaluated by scratch test indicates that the adhesion strength of HA coating was improved with the presence of titania interlayer.

## 1 Introduction

Calcium phosphate ceramics particularly hydroxyapatite has gained much interest among material scientists as well as medical practitioners as synthetic bone substitutes. Even though these are already being used as fillers for treating various bone defects, their application is limited in non-load bearing uses due to brittle fracture of ceramic components [1–6]. On the other hand, because of the better physico-chemical, mechanical and biological properties, titanium and its alloys are extensively used for load bearing applications such as bone plates, screws, and artificial joints. A number of titanium based implants with bioactive ceramic coating around the bone contacting areas are available in the market. This is to accelerate the osteo-integration, which help the patient to faster rehabilitation. An adherent bioactive ceramic coating was preferred to have a faster bone-implant bonding, there by reducing the post implantation healing time which provides long term *in vivo* functionality [7–13]. Among the various techniques such as sol-gel coatings, electro deposition, dip coating, ion beam and various other vapor deposition processes, plasma spraying is the commercially viable technique for clinical application. Despite its ability to produce various bioactive ceramic coating with high coating adhesion strength, there are many demerits for plasma spray such as variable crystalline nature and chemical inhomogeneity in coating [14–16].

Pulsed Laser Deposition (PLD) technique has been evolved as an alternative to aforesaid methods and has an added advantage of preservation of stoichiometry of target phase. PLD technique also possesses the ability to form desired film thickness, morphology and composition by varying the deposition parameters. This method additionally provides deposition of different target materials of unique physico-chemical and biological properties over

P. Rajesh · M. Komath · H. Varma (✉)  
Bioceramics Laboratory, Biomedical Technology Wing, Sree Chitra Tirunal Institute for Medical Sciences and Technology (SCTIMST), Trivandrum, Kerala 695012, India  
e-mail: varma@sctimst.ac.in; prhkvarma@gmail.com

C. V. Muraleedharan  
Division of Artificial Internal Organs, Biomedical Technology Wing, Sree Chitra Tirunal Institute for Medical Sciences and Technology (SCTIMST), Trivandrum, Kerala 695012, India

single substrate for functionally graded coatings [16–20]. Many in vivo studies have reported that HA-coated Ti had enhanced implant fixation within a period of 3–6 months [9–13]. However, certain difficulties such as maintenance of phase purity and mechanical strength in vivo, have been encountered in many of the coating techniques including the plasma-sprayed coatings. Titanium has also shown to possess inherent biocompatibility as it forms a thin  $\text{TiO}_2$  layer of several nanometres which easily forms under normal atmospheric conditions [21, 22]. Reports have shown that an interlayer of titania ( $\text{TiO}_2$ ) formed by methods like sol-gel can improve the coating adhesion between the HA and Ti substrate [22–24]. In the present work an attempt has been made to improve the mechanical property of hydroxyapatite coating on titanium substrate by incorporating a titania interlayer by making use of PLD for multi-target deposition, since the deposited interlayer helps to improve the coating adhesion strength as well as maintains the target stoichiometry.

## 2 Materials and methods

### 2.1 Preparation of target materials

#### 2.1.1 Preparation of dense HA target

Hydroxyapatite (HA) powder was synthesized by a wet precipitation method involving calcium nitrate and ammonium dihydrogen phosphate (Rankem, India) in stoichiometric proportions at a pH of 11 at 80°C [25]. The precipitate was aged in the mother liquor for 24 h, washed with distilled water to get rid of surface impurities such as nitrates and ammonium ions. The filter cake obtained was freeze-dried, calcined at 300°C for 2 h, pulverised and sieved to get HA particles having a uniform size in the range of 125 µm. HA powder was then compacted to 30 mm diameter and 5 mm thick discs by isostatic pressing at a pressure of 80 MPa (Cold Isostatic Press, EPSI, Belgium). The discs were sintered at 1100°C for 2 h. The density of the sintered disc was measured by Archimedes method and was found to be 3.07 g/cm<sup>3</sup>. Sintered discs were mechanically polished (Buehler-Ecomet 3 Variable speed Grinder-Polisher, Buehler Ltd, U.S.A) with a series of SiC papers having grit size ranging from 320 to 800 to get uniform surface. The discs were then cleaned ultrasonically in distilled water, rectified spirit and finally in acetone. The cleaned substrates were then dried by blowing hot air around 70°C.

#### 2.1.2 Preparation of titania ( $\text{TiO}_2$ —rutile) target

Commercial Titanium dioxide (Rutile) (SD Fine Chem. Ltd., India) powder was compacted by isostatic press

similar to that of HA but by adding 5% poly vinyl alcohol as binder.  $\text{TiO}_2$  discs were made of the same dimension as that of HA disc. The compacted discs were sintered at 1230°C for 10 h. Surface was then polished and cleaned as stated for HA discs.

### 2.2 Preparation of substrate material—titanium disc

Commercially available Ti6Al4V sheet (ASTM F1108, Manhar Metal Supply Corporation, Mumbai, India) were machined into 15 mm × 20 mm size and were mechanically polished through a series of SiC papers to have uniform surface. These substrates are cleaned ultrasonically in distilled water, rectified spirit and finally in acetone.

### 2.3 Pulsed laser deposition

A custom designed pulsed laser deposition system was used for the present study (fabricated by Excel Instruments, Mumbai, India). The system consists of a stainless steel vacuum chamber evacuated by a turbo molecular pump backed with a rotary vane pump. A pirani and cold cathode gauge were used to measure the total pressure of the vacuum chamber. Chamber was also equipped with high temperature substrate holder where the substrate can be heated up to a maximum of 800°C which is programmed with the attached temperature controller and readout unit. The deposition system utilized high power Q-switched Nd-YAG laser (Quanta System S.P.A, Italy). In these experiments the radiation of the third (355 nm) harmonics with a repetition rate of 10 Hz and pulse width of 6–8 ns were used. The output laser beam of 2 W power was focussed to a spot size of about 2 mm with a spherical lens on to the HA target fixed at an angle of 45° with respect to incident beam. The target and substrate holder were set parallel and the distance between them was fixed at 35 mm. Before deposition the chamber was evacuated to a pressure of the order of 10<sup>-6</sup> mbar and then filled with oxygen to an optimized working gas pressure of 1 mbar for the deposition of  $\text{TiO}_2$  and 1 × 10<sup>-3</sup> mbar for the deposition of HA. The oxygen pressure was controlled by a needle valve. The targets were rotated by means of attached DC motor during deposition so as to eliminate depletion of material at one point and thereby maintains a uniform fresh surface for each incoming laser pulse. The substrate temperature was previously optimized for better coating properties and kept at 400°C. Different targets were ablated for different time periods depending on the deposition parameters and to have different coating thickness. HA coating with and without  $\text{TiO}_2$  were then analysed for various physicochemical and mechanical characteristics.

## 2.4 Material characterization

### 2.4.1 Profilometry

The surface roughness of Ti6Al4V substrate, coating thickness of  $\text{TiO}_2$  layer and that of  $\text{TiO}_2\text{-HA}$  coating on titanium substrate were measured by profilometry technique. The surface profile was obtained using TalySurf CLI 1000 (Taylor Hobson, UK) with the software Talymap Gold (version 4.1). A surface of  $15 \text{ mm} \times 10 \text{ mm}$  containing both coated and uncoated region was scanned at  $50 \mu\text{m}/\text{s}$  speed,  $0.5 \mu\text{m}$  spacing, and  $100 \text{ Hz}$  sampling rate. The thickness of the coating was also determined by step height measurement.

### 2.4.2 X-ray diffraction analysis

The phase and crystallinity analysis of both targets and the deposited films were done by X-ray diffraction technique. The samples were scanned using  $\text{Cu K}\alpha$  radiation at a voltage of  $40 \text{ kV}$  and a current of  $30 \text{ mA}$  (Siemens D-5005 X-ray Diffractometer, Germany) in the  $2\theta$  range  $10\text{--}70^\circ$  in the case of targets and  $20\text{--}50^\circ$  for the coated specimens to avoid intense substrate peaks.

### 2.4.3 Fourier transform infrared spectroscopy (FTIR)

FTIR analysis was performed on a Thermo Nicolet 5700 spectrometer (USA) and the spectra were collected in the diffuse reflectance (DRIFT) mode. Spectra of targets and the coating obtained were compared. Samples were prepared by mixing the target powder with optical grade KBr powder; while pure KBr was used as the background. The samples of the coating were collected by scratching the surface. The spectra were recorded at an average number of 64 scans between  $400$  and  $4000 \text{ cm}^{-1}$  and at a resolution of  $4 \text{ cm}^{-1}$ .

### 2.4.4 Scanning electron microscopy and energy-dispersive X-ray analysis (SEM-EDS)

The coatings obtained were compared with the targets for the elemental composition and microstructural morphology by an environmental scanning electron microscope (ESEM-Quanta 200, Germany) equipped with an energy-dispersive X-ray analysis device (EDAX; OXFORD, X-ray microanalysis software). SEM was also used to examine the failure mode of HA coating after performing the scratch test. The samples were examined as such at low vacuum mode without any coating.

### 2.4.5 Inductively coupled plasma-optical emission spectrometry (ICP-OES)

The elemental analysis for determining Ca/P ratio of the HA target as well as the coating was done by an ICP-OES (Perkin Elmer 5300 DV, USA). Sample solutions were prepared by dissolving in 5%  $\text{HNO}_3$ . The analysis was carried out with a calibration plot of known standards and the experiments were done in triplicate.

### 2.4.6 Micro-scratch testing

The mechanical properties of the different coatings were compared with a micro-scratch tester (Micro-combi tester; CSM Instruments, Switzerland). The scratch test was performed with reference to ISO 20502:2005(E) [26]. A diamond tip of  $100 \mu\text{m}$  (Rockwell) was used for the scratch test and the scratch track was examined with an attached optical microscope and further by ESEM. The scratch tip was moved under a progressive loading rate of 3.95 and  $9.97 \text{ N/min}$  respectively for HA and  $\text{TiO}_2\text{-HA}$  coatings through a scratch length of  $10 \text{ mm}$ . Both frictional force and acoustic emission was measured to derive a conclusion of coating failure.

## 3 Results and discussion

### 3.1 Characterisation of targets and substrate

The sintered HA discs were analysed for phase and composition by XRD, FTIR and ICP while that of  $\text{TiO}_2$  by XRD prior to use as targets for the PLD. Figure 1 shows the XRD patterns of the Ti6Al4V substrate, HA and  $\text{TiO}_2$  targets. All the three patterns correspond to JCPDS patterns 44-1294 (Ti-substrate), 9-0432 (HA-target), and 21-1276 ( $\text{TiO}_2$ -rutile target). The crystallite size was found to be in the range of  $40\text{--}45 \text{ nm}$  for the sintered HA target and  $5\text{--}10 \text{ nm}$  in the case of  $\text{TiO}_2$  target as measured by the Scherer equation. Both the target samples were identified as highly crystalline and phase pure without any additional phases within the detection limit.

FTIR spectra of HA target is shown in Fig. 2. The spectrum of HA target is similar to that of a synthetic hydroxyapatite illustrating various peaks correspond to hydroxyl and phosphate groups. Hydroxyl stretching is observed at  $3570.3 \text{ cm}^{-1}$  in the spectra of sintered HA target. All the theoretically predicted vibrational modes for phosphate group  $v_1$  to  $v_4$  were present in the prepared HA. The different sites present in the region  $1090\text{--}970 \text{ cm}^{-1}$  confirms hydroxyapatite rather than a carbonated hydroxyapatite which if present should have only a single

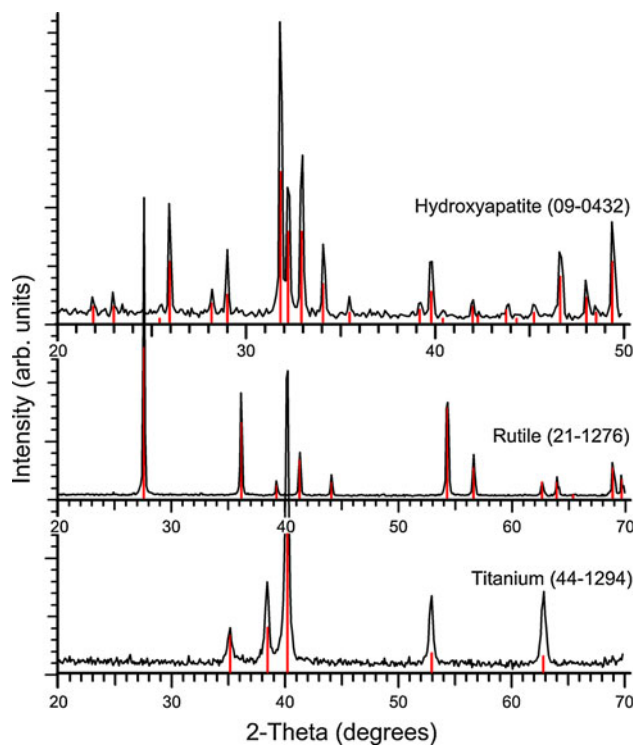


**Fig. 1** XRD patterns of the Ti6Al4V substrate, sintered  $\text{TiO}_2$  and HA targets along with standard patterns

peak for phosphate  $\nu_3$  band centred around  $1046\text{ cm}^{-1}$ . Band at  $962.4\text{ cm}^{-1}$  is the phosphate  $\nu_1$  band and  $\nu_4$  bands is observed in the region  $660\text{--}520\text{ cm}^{-1}$  and the presence of three sites at  $629.9$ ,  $600.7$ , and  $571.3\text{ cm}^{-1}$  strongly indicate non-carbonated HA rather than carbonated HA

**Fig. 2** FTIR spectrum of sintered HA target used for PLD

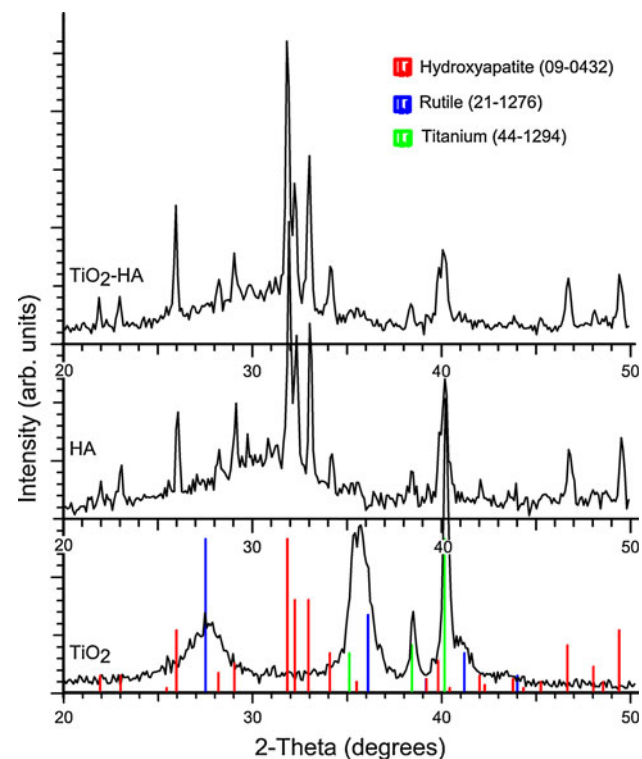
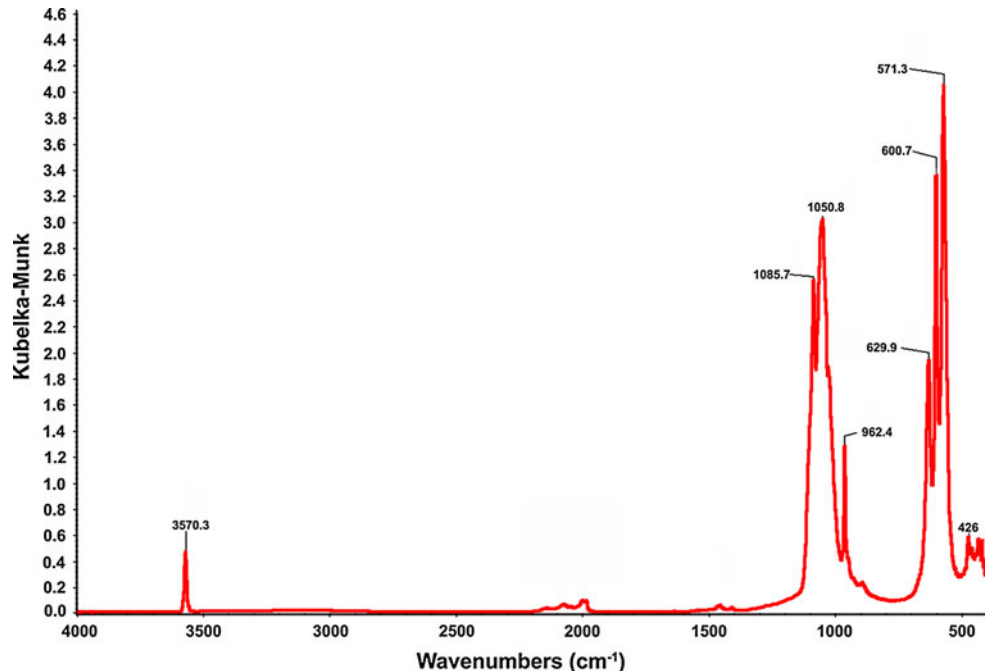


**Fig. 3** XRD patterns of pulsed laser deposited  $\text{TiO}_2$ , HA and  $\text{TiO}_2$ -HA

which would have only two sites. There also present the usually weak phosphate  $\nu_2$  bands in the region  $475\text{--}450\text{ cm}^{-1}$  [27]. Presence of these characteristic groups ensures the use of phase pure synthetic HA as the target for PLD.

The Ca/P ratio of the sintered HA as determined by ICP was  $1.64 \pm 0.02$  which is close to the expected stoichiometric (1.67) HA. These results obtained from XRD, FTIR and ICP clearly ensures use of stoichiometric, highly crystalline HA and  $\text{TiO}_2$  as targets for PLD.

The Ti6Al4V alloy being used as the substrate for HA deposition, were analyzed for their average surface roughness to ensure the use of uniform surface profile and was found to be  $0.25 \mu\text{m}$ .

### 3.2 Characterization of coating

The coating thickness of individual layers was assessed separately; thickness of  $\text{TiO}_2$  coating alone was found to be around 200 nm. The HA coating with  $\text{TiO}_2$  interlayer is found to have an approximate thickness of 1 micron. Figure 3 shows the XRD patterns of the three coatings  $\text{TiO}_2$ , HA and  $\text{TiO}_2$ -HA. The patterns were compared with JCPDS files and shows that  $\text{TiO}_2$  coating matches with the rutile phase (JCPDS No. 21-1276) with a (110) orientation. The intensity of the  $\text{TiO}_2$  rutile peaks was comparatively lower because of the intense peaks of titanium substrate while the broader nature of peaks was due to the nano crystallite size. XRD pattern of HA coating exactly matches with JCPDS file No. 9-432 with the same (211) orientation of HA target and indicates phase pure composition of coating without any additional calcium phosphate phases at least within the detection level. The pattern of HA coating with  $\text{TiO}_2$  interlayer also seems to be same as that with out interlayer but the increased peak intensity and

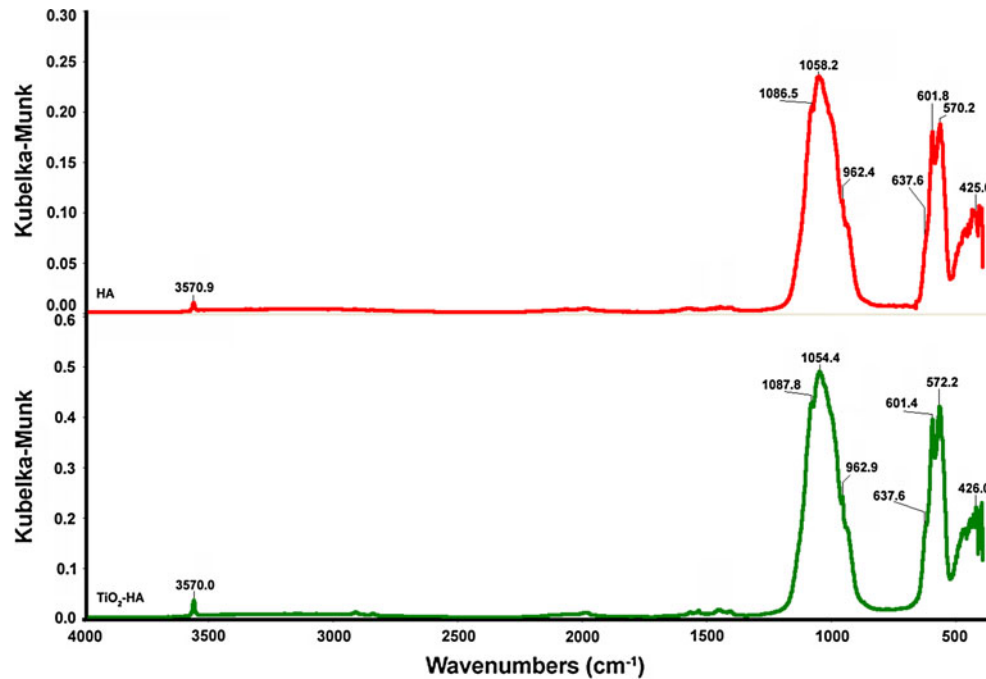
sharpness obtained were attributed to improved crystallinity of HA with  $\text{TiO}_2$  interlayer.

FTIR analysis results for the HA and  $\text{TiO}_2$ -HA preparations are depicted in Fig. 4. Both the spectra obtained are similar except the increased intensity obtained for  $\text{TiO}_2$ -HA coating compared to HA coating. After laser ablation, the spectra obtained revealed no significant changes in the positions of various functional group frequencies. Hydroxyl ( $-\text{OH}$ ) peak was still present around  $3570 \text{ cm}^{-1}$ , indicating that the  $-\text{OH}$  group in the HA structure was well preserved after laser ablation but the peak intensity lost to some extent. The peak area and intensity of phosphate group were relatively different from the target probably because of the sample preparation i.e., from bulk HA and from surface of coating and else due to the less crystalline nature of HA coating compared to target powder. Although the spectra of coating gives only less resolved peak splitting, phosphate bands is having the same splitting pattern in both the target and coating indicates the similar site symmetry of phosphate group [20, 27, 28].

The Ca/P ratio for the HA and  $\text{TiO}_2$ -HA coatings determined by elemental analysis performed by ICP was found to be  $1.64 \pm 0.02$  indicates preservation of Ca/P stoichiometry in both the coatings.

Scanning electron microscopy analysis performed on the deposited samples, together with elemental analysis by EDS, provided supplementary information regarding the chemical composition and the morphological structure of the deposits. Figures 5, 6 and 7 shows the micro-structural features of  $\text{TiO}_2$ , HA and that of HA coating with  $\text{TiO}_2$

**Fig. 4** FTIR spectra of pulsed laser deposited HA coating on Ti6Al4V substrate (HA) without  $\text{TiO}_2$  and with  $\text{TiO}_2$  interlayer (TiO<sub>2</sub>-HA)



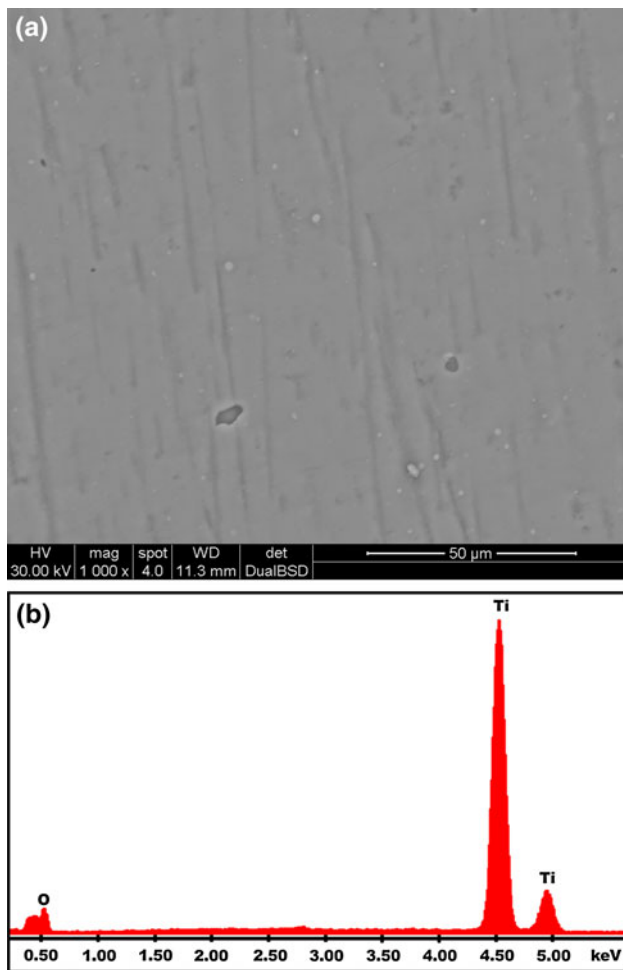


**Fig. 5** SEM image of  $\text{TiO}_2$  coating on  $\text{Ti}6\text{Al}4\text{V}$  substrate (a) and the corresponding EDS pattern (b)

interlayer respectively. The EDS analysis shows the presence of Ca, P, O and Ti peaks according to their elemental composition in the coatings and indicates the presence of  $\text{TiO}_2$  and calcium phosphates on the substrate as expected. The deposited  $\text{TiO}_2$  cannot be distinguished easily because of the small coating thickness and high uniformity. But the HA coatings have grown to form thick layer with particles bound together during the film growth process. The HA coating with  $\text{TiO}_2$  interlayer (Fig. 7) is more uniform with very few grooves and pinholes when compared to HA coating with out interlayer (Fig. 6). Similar EDS spectra was obtained for both type of coating and Fig. 7c is the EDS spectra indicating the presence of Ca, P, O, and Ti on the surface of the HA coating with titania interlayer. The higher magnification SEM micrograph shows that HA particles deposited are grown to form clusters and further seems to form a dense aggregated structure on the substrate with the interlayer.

The scratch test performed gave the acoustic and frictional force along with the penetration depth. Figure 8

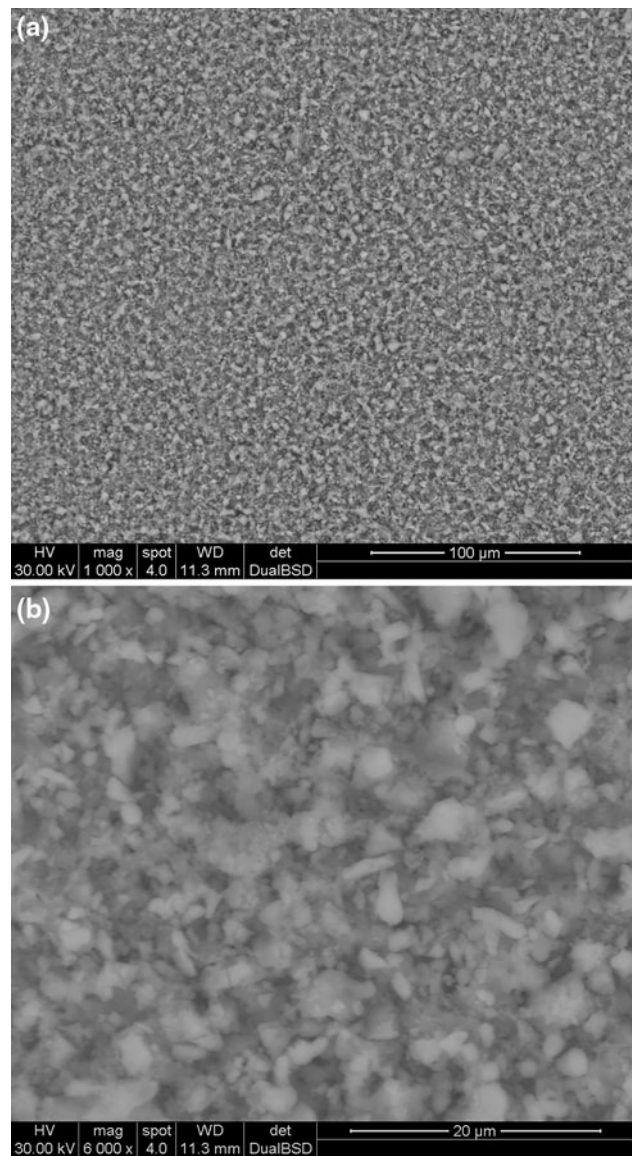


**Fig. 6** SEM images of HA coating on  $\text{Ti}6\text{Al}4\text{V}$  substrate (a) at lower magnification and (b) at higher magnification

shows the representative acoustic emissions produced during the scratch test for both the HA coatings i.e., with and without  $\text{TiO}_2$  interlayer. Different failure modes and points were assigned in the acoustic profile by observed through the attached optical image capturing device and are denoted in the figure as first crack, first delamination and finally as point of complete delamination of the coated layer. SEM of crack initiation (marked by arrows) and area of complete delamination are also shown respectively in Fig. 9a, b. In the case of HA coating without interlayer (Fig. 8a), the first crack was formed around 0.82 N, and there is a gradual ploughing of HA coating even at lower loads which leads to the first delamination of coating at 1.46 N. As the load increases further, the width and depth

**Fig. 7** SEM images of HA coating on Ti6Al4V substrate with  $\text{TiO}_2$  interlayer **(a)** at lower magnification **(b)** higher magnification. **(c)** Energy dispersive spectrum of HA coating on Ti6Al4V substrate with  $\text{TiO}_2$  interlayer

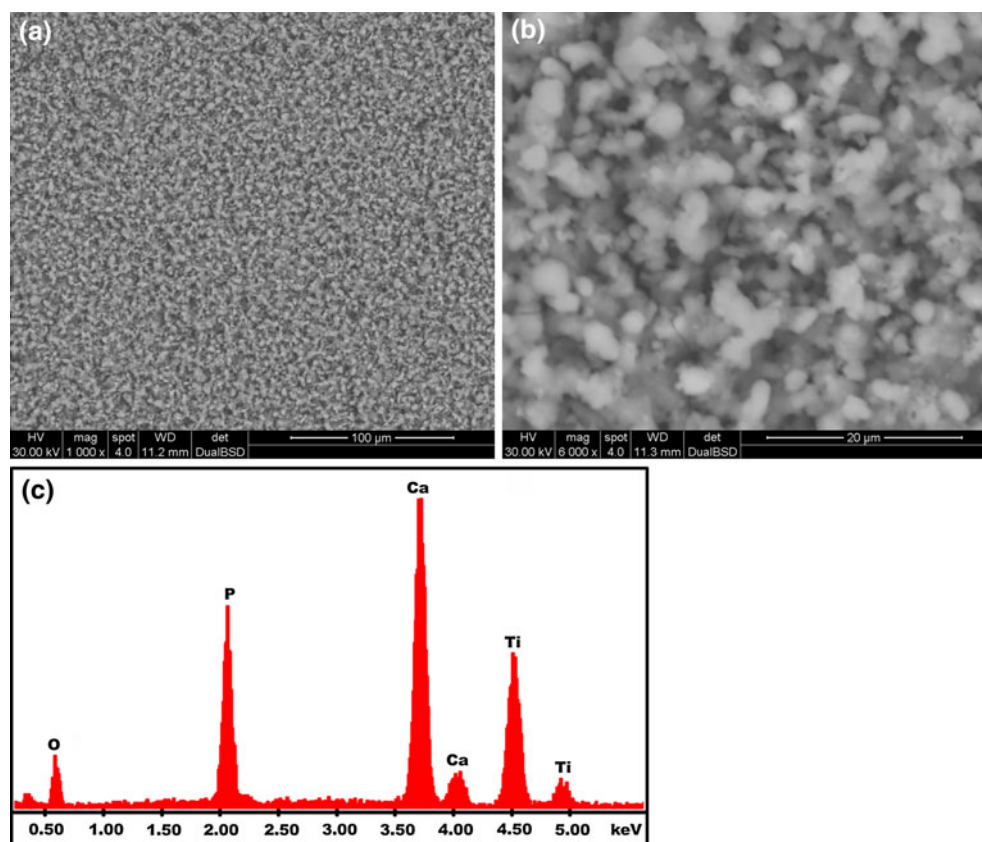
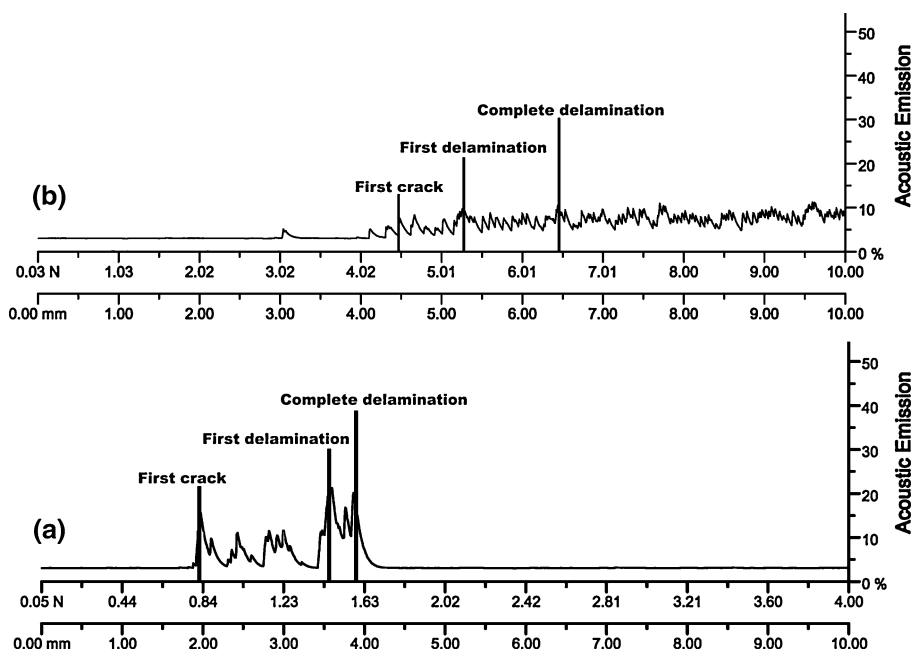


**Fig. 8** Acoustic emission profile of scratch test **(a)** HA coating on Ti6Al4V substrate **(b)** HA coating on Ti6Al4V substrate with  $\text{TiO}_2$  interlayer



of scratch increases till the indenter reaches the metal surface. At this point (1.59 N); there is an abrupt increase in the acoustic signal and further remains stable for the metallic surface. It was also confirmed by SEM and EDS that there is still a thin calcium phosphate layer in the scratch groove which may be carried by the scratch tip and

by spallation from the scratch edges till the point where complete delamination occurs. Coating failure was mainly due to the substrate coating interface and the low internal cohesion within the coating. The behaviour of acoustic emission is quite different for the coating with  $\text{TiO}_2$  interlayer Fig. 8b. Here there is no such detachment of

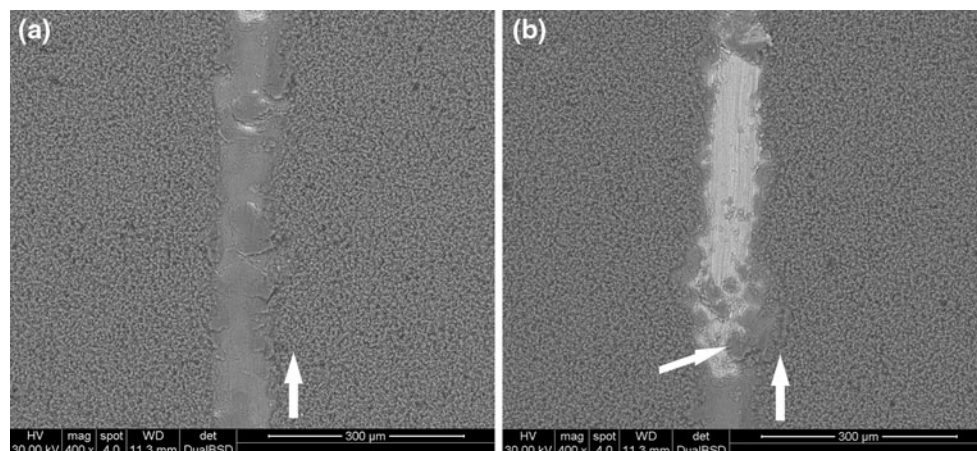


**Fig. 9** SEM images of HA coating after scratch test showing (a) direction of scratch test with area of crack initiation and (b) region of complete delamination indicated by arrow

layer at lower loads and the coating first fails within itself at about 4.48 N and on further increase of load up to 5.29 N the coating seems to be adhered well to the substrate. Beyond 6.46 N there is an increase in penetration depth with normal deflection in acoustic signal, which is due to complete removal of HA layer and substrate penetration. But the nature of acoustic emission compared to that of HA single layer conveys that the interlayer and HA adhered well each other and to the substrate so that there is no sign of abrupt coating failure. Here there is no single point observed where the coating got detached completely from the substrate; rather the coating and substrate seems to behave as a single layer with an adherent interlayer. Hence the thin TiO<sub>2</sub> coating provided seems to act as the binding layer between the titanium and HA layer.

#### 4 Conclusions

The Pulsed Laser Deposition (PLD) technique is highly advantageous for obtaining stoichiometric and adherent HA coatings over titanium substrate. The ability of PLD to deposit multi-targets is used to provide an interlayer of TiO<sub>2</sub> and is found to be very promising for obtaining improved bonding strength of HA coating onto titanium substrate. The XRD, FTIR, SEM and ICP analysis confirmed the formation of HA coating without any other phases even with the interlayer. Comparison of the mechanical property of HA coating with TiO<sub>2</sub>-HA clearly demonstrates the improved adhesion of coating by incorporating an interlayer of titania. Thus implants making use of HA coating can be further improved by providing an adequate interlayer for their *in vivo* functionality and long term performance.

**Acknowledgments** The authors gratefully acknowledge The Director and Head, Biomedical Technology Wing, Sree Chitra

Tirunal Institute for Medical Sciences and Technology (SCTIMST) for extending the research facilities to successfully carry out this work. Rajesh P acknowledges Kerala State Council for Science Technology and Environment (KSCSTE) for the research fellowship.

#### References

1. Hench LL. Bioceramics: from concept to clinic. *J Am Ceram Soc*. 1991;74(7):1487–510.
2. Legeros RZ. Calcium phosphate materials in restorative dentistry: a review. *Adv Dent Res*. 1988;2(1):164–80.
3. Navarro M, Michiardi A, Castano O, Planell JA. Biomaterials in orthopaedics. *J R Soc Interface*. 2008;5:1137–58. doi:[10.1098/rsif.2008.0151](https://doi.org/10.1098/rsif.2008.0151).
4. Menon KV, Varma HK. Radiological outcome of tibial plateau fractures treated with percutaneously introduced synthetic porous hydroxyapatite granules. *Eur J Orthop Surg Traumatol*. 2005;15: 205–13. doi:[10.1007/s00590-005-0238-6](https://doi.org/10.1007/s00590-005-0238-6).
5. John Annie, Varma HK, Kumari TV. Surface reactivity of calcium phosphate based ceramics in a cell culture system. *J Biomater Appl*. 2003;18:63–78. doi:[10.1177/0885328203018001006](https://doi.org/10.1177/0885328203018001006).
6. Anil Kumar PR, Varma HK, Kumary TV. Rapid and complete cellularization of hydroxyapatite for bone tissue engineering. *Acta Biomater*. 2005;1(5):545–52. doi:[10.1016/j.actbio.2005.05.002](https://doi.org/10.1016/j.actbio.2005.05.002).
7. De Groot K, Wolke JGC, Jansen JA. Calcium phosphate coatings for medical implants. *Proc Instn Mech Engrs, Part H*. 1998;212(2): 137–47. doi:[10.1243/0954411981533917](https://doi.org/10.1243/0954411981533917).
8. Lacefield William R. Material characteristics of uncoated/ceramic-coated implant materials. *Adv Dent Res*. 1999;13:21–6. doi:[10.1177/0885328203018001001](https://doi.org/10.1177/0885328203018001001).
9. Overgaard S, Bromose U, Lind M, Bunger C, Soballe K. The influence of crystallinity of the hydroxyapatite coating on the fixation of implants- Mechanical and histomorphometric results. *J Bone Joint Surg [Br]*. 1999;81-B:725–31.
10. Slack R, Tindall A, Shetty AA, James KD, Rand C. 15-year follow-up results of hydroxyapatite ceramic-coated femoral stem. *J Orthop Surg*. 2006;14(2):151–4.
11. Landor Ivan, Vavrik Pavel, Sosna Antonin, Jahoda David, Hahn Henry, Daniel M. Hydroxyapatite porous coating and the osteointegration of the total hip replacement. *Arch Orthop Trauma Surg*. 2007;127:81–9. doi:[10.1007/s00402-006-0235-1](https://doi.org/10.1007/s00402-006-0235-1).

12. Fish JM, Misch CE. Mandibular bone growth induced by a hydroxyapatite-coated subperiosteal implant: a case report. *J Oral Implantol.* 2000;26(4):267–75.
13. Placzek R, Ruffer M, Deuretzbacher G, Heijens E, Meiss AL. The fixation strength of hydroxyapatite-coated Schanz screws and standard stainless steel Schanz screws in lower extremity lengthening. *Arch Orthop Trauma Surg.* 2006;126:369–73. doi: [10.1007/s00402-006-0142-5](https://doi.org/10.1007/s00402-006-0142-5).
14. Wen J, Leng Y, Chen J, Zhang C. Chemical gradient in plasma-sprayed HA coatings. *Biomaterials.* 2000;21:1339–43.
15. Yan L, Leng Y, Weng L-T. Characterization of chemical inhomogeneity in plasma-sprayed hydroxyapatite coatings. *Biomaterials.* 2003;24:2585–92.
16. Garcia Sanz FJ, Mayor MB, Arias JL, Pou J, Leon B, Perez Amor M. Hydroxyapatite coatings: a comparative study between plasma-spray and pulsed laser deposition techniques. *J Mater Sci Mater Med.* 1997;8:861–5.
17. Bao Q, Chen C, Wang D, Ji Q, Lei T. Pulsed laser deposition and its current research status in preparing hydroxyapatite thin films. *Appl Surf Sci.* 2005;252:1538–44.
18. Bigi A, Bracci B, Cuisinier F, Elkaim R, Fini M, Mayer I, Mihailescu IN, Socol G, Sturba L, Torricelli P. Human osteoblast response to pulsed laser deposited calcium phosphate coatings. *Biomaterials.* 2005;26:2381–9.
19. Fernandez Pradas JM, Garcia Cuenca MV, Cleries L, Sardin G, Morenza JL. Influence of the interface layer on the adhesion of pulsed laser deposited hydroxyapatite coatings on titanium alloy. *Appl Surf Sci.* 2002;195:31–7.
20. Zeng H, Lacefield WR. XPS, EDX and FTIR analysis of pulsed laser deposited calcium phosphate bioceramic coatings: the effects of various process parameters. *Biomaterials.* 2000;21:23–30.
21. Feng B, Weng J, Yang BC. Characterization of surface oxide films on titanium and adhesion of osteoblast. *Biomaterials.* 2003;24:4663–70.
22. Ergun C, Doremus R, Lanford W. Hydroxylapatite and titanium: interfacial reactions. *J Biomed Mater Res.* 2003;65A:336–43.
23. Kim HW, Koh YH, Li LH, Lee S, Kim HE. Hydroxyapatite coating on titanium substrate with titania buffer layer processed by sol–gel method. *Biomaterials.* 2004;25:2533–8.
24. Lee SH, Kim HW, Lee EJ, Li LH, Kim HE. Hydroxyapatite– $TiO_2$  hybrid coating on Ti implants. *J Biomater Appl.* 2006;20:195–208. doi: [10.1177/0885328206050518](https://doi.org/10.1177/0885328206050518).
25. Varma HK, Sivakumar R. Preparation and characterisation of free flowing hydroxyapatite powders. *Phosphorous Res Bull.* 1996;6: 35–8.
26. ISO 20502:2005(E). Fine ceramics (advanced ceramics, advanced technical ceramics)—determination of adhesion of ceramic coatings by scratch testing. Geneva, Switzerland: International organization for standardization ISO.
27. Rehman I, Bonfield W. Characterization of hydroxyapatite and carbonated apatite by photo acoustic FTIR spectroscopy. *J Mater Sci Mater Med.* 1997;8:1–4.
28. Rau JV, Nunziante Cesaro S, Ferro D, Barinov SM, Fadeeva IV. FTIR study of carbonate loss from carbonated apatites in the wide temperature range. *Biomed Mater Res Part B Appl Biomater.* 2004;71B:441–7. doi: [10.1002/jbm.b.30111](https://doi.org/10.1002/jbm.b.30111).